

# Calibration concept for potential optical aberrations of the APEX pushbroom imaging spectrometer

Daniel Schläpfer, Johannes W. Kaiser, Jason Brazile, Michael Schaepman, and Klaus I. Itten  
Remote Sensing Laboratories, University of Zürich, Winterthurerstr. 190, CH-8057 Zürich,  
Switzerland

## ABSTRACT

The high resolution airborne imaging spectrometer APEX (Airborne Prism Experiment) is currently being built. In parallel, its data processing calibration chain is being designed. The complex design of this high resolution pushbroom instrument bears the risk of optical aberrations in the registered spatio-spectral frames. Such aberrations consist of so-called frown and smile effects, as well as ghost image, smear, and stray light contributions. A concept is presented which shall operationally improve image calibration by inversion of the sensor model.

**Keywords:** calibration, imaging spectroscopy, pushbroom sensor, hyperspectral, optical aberrations

## 1. INTRODUCTION

The high resolution airborne imaging spectrometer APEX (Airborne Prism Experiment) is currently being built in a joint Swiss/Belgium project funded through ESA.<sup>1,2</sup> This instrument is constructed as an airborne dispersive pushbroom instrument having 1000 pixels across track and more than 300 spectral bands registered simultaneously on two distinct detector arrays. The development of an appropriate calibration chain for this kind of instrument is a challenging endeavour. Expected optical aberrations in the registered spatio-spectral frames are so-called frown and smile effects,<sup>3</sup> as well as ghost image and stray light contributions.

In this paper, the data correction scheme and the underlying instrument forward model is depicted. An integral but simple forward model is used to model the sensor data readouts based on at-sensor radiance values. It combines optical effects with detector and electronics response. This model helps to define the parameters required for data calibration. The inversion of the forward model leads to a correction scheme for acquired digital image data which bases on the concept proposed by Schläpfer et al.<sup>4</sup> Image-frame based correction algorithms are designed in a way to correct optical aberrations efficiently on a limited number of recorded frames, while the radiometric response can be corrected on a per-pixel basis. An implementation scheme is furthermore required which allows for fast computation of the correction functions and for production of radiometrically improved calibrated data products.

A trade-off between the real-world performance of the instrument and the individual steps to be included in the APEX standard processing chain will only be possible upon availability of APEX, scheduled for mid 2005. Nevertheless, recommendations on priorities for the data calibration process can already be made based on the currently expected instrument performance.

## 2. COORDINATE SYSTEM DEFINITIONS

The calibration of airborne imaging spectroscopy detector readouts to consistent coordinates in object space can be modeled as transformation between a series of coordinate systems. Figure 1 gives an overview of coordinate systems used for the setup of the sensor model.

The raw measurements are acquired and stored in detector space coordinates. A digital number (DN) is registered in each detector pixel as  $DN_{i,j,k}$ . The integer-type indices denote:

$i$  : pixel index in along track dimension,

---

author contact information: E-mail: dschlapf@geo.unizh.ch, Telephone: +41 1 635 52 50

$j$  : pixel index in spectral dimension, and

$k$  : pixel index in across-track dimension.

The original order of these indices may be arbitrary due to the detector readout process, but may be re-sorted in ascending order. For the APEX sensor, a re-sort in ascending wavelength order per detector array is planned as a transformation within detector space.

The transformation of detector space to image space is covered by radiometric calibration. In image space, the real dimensions of the detector array and the distortion in the imaged data are governing all optical aberrations. The dimensions in image space are given as:

$x, t$  : along track or temporal dimension,

$y$  : image position on detector in spectral dimension,

$z$  : image position on detector in across-track dimension.

This coordinate system is usually used for optical modeling in sensor construction and as a basis in laboratory calibration.

After data calibration, the relation between sensor measurements and object space is found. The radiance field at the sensor entrance is sampled to  $L_s(t, \lambda, \theta)$  [ $W/(m^2 sr nm)$ ], where

$t$  : time of data registration (middle of integration time),

$\lambda$  : band central wavelength, and

$\theta$  : across-track pixel view angle at pixel center.

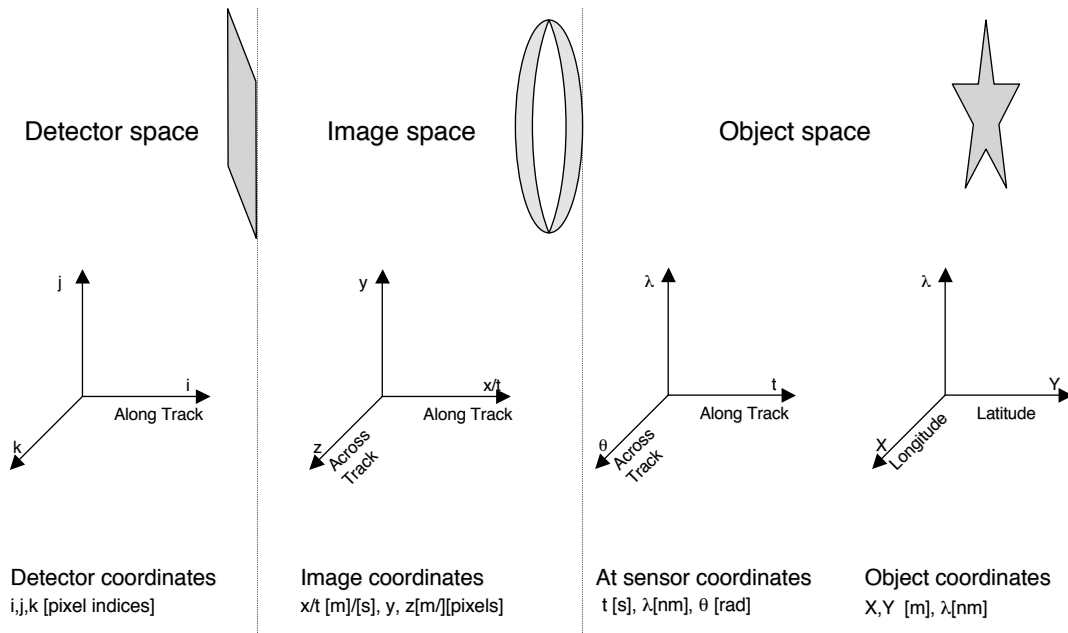


**Figure 1.** Coordinate systems used in the APEX data calibration algorithms.

This representation together with the knowledge of sensor position  $(x_S, y_S, z_S)$ , attitude angles  $(\omega, \varphi, \kappa)$  and the internal sensor geometry describes the full object space geometry.

In calibrated imaging spectroscopy data, consistency in the latter coordinate system is expected. The dimensions of a 3-dimensional imaging spectroscopy cube correspond to the parameters time, central wavelength position, and across track view angle. Additionally, the response curves in these three directions are associated in a 1:1 manner for each pixel, being constant within the required accuracy with respect to the non-associated dimension (eg; the spectral response shall be constant with time and across track view angle).

For application of the data in mapping and geographic information science, a final transformation within object space is required ending up at orthographic object coordinates:

$X$  : geographical longitude or local X coordinate,

$Y$  : geographical latitude or local Y coordinate, and

$\lambda$  : nominal band center wavelength

The latter transformation is not part of Level 1 processing in the APEX processing chain but will be done using dedicated software (e.g., PARGE<sup>5</sup>) as part or option of Level 2 processing.

### 3. SENSOR FORWARD MODEL

For proper inversion and correction of radiometric effects and for testing of the developed procedures, an appropriate forward model describing the whole sensor system has to be described in detail and implemented. Three distinct steps are separated:

- Optical model: describing optical aberrations between at-sensor radiance and detector.<sup>3</sup>
- Bad pixels: loss of information during data registration due to bad pixels<sup>6</sup> and other effects such as saturation.
- Radiometric model: transformation of at-detector photon flux to stored digital numbers.

Below, the forward formulations of these three steps are given, while the inversion approaches are described in the subsequent section.

#### 3.1. Optical Model

The optical forward model incorporates three distinct steps: first the wavelength and angular coordinates are calculated for all detector pixels. By adding the stray light contribution, the at-sensor radiance field is then derived. This field is sampled at the calculated coordinates to obtain the photon fluxes at detector, and finally the convolution of the calculated photon flux at detector with the optics PSF is incorporated.

##### 3.1.1. Coordinate Transformation

The coordinate systems of detector pixels indices  $j$  and  $k$  and the one of wavelength length  $\lambda$  and across-track angle  $\theta$  are shown in Figure 1. Parameterizing the transformation models the spectral and spatial behavior of the instrument as well as its smile and frown. A parameterization with 2-dimensional 2nd order polynomials is used in a first order of approximation:

$$\lambda(y, z) = a_0^\lambda + a_1^\lambda y + a_2^\lambda z + a_3^\lambda y^2 + a_4^\lambda z^2 + a_5^\lambda yz \quad (1)$$

$$\theta(y, z) = a_0^\theta + a_1^\theta y + a_2^\theta z + a_3^\theta y^2 + a_4^\theta z^2 + a_5^\theta yz \quad (2)$$

This formulation describes the projection of  $(\lambda, \theta)$  in image space to  $(y, z)$ . After characterization of the actual instrument another parameterization might be substituted for the polynomial.

### 3.1.2. Radiance Sampling

Once the coordinate transformation is established, the radiance values in the old coordinate system need to be mapped to values of “pixels” in the detector coordinate system. The problem is that in general a position in the image coordinate system does not map directly to one in the other coordinate system. Therefore, the mapped values must be synthesized from neighboring “pixels” in the image space coordinate system.

The radiance at sensor is given in a matrix with specified  $\lambda$  and  $\theta$  values. It is used as a look-up table (LUT) for evaluating the radiance at sensor for arbitrary  $\lambda$  and  $\theta$  values:

$$L_s(j, k) = L_s(\lambda(y_j, z_k), \theta(y_j, z_k)) \quad , \quad (3)$$

where  $\lambda$  and  $\theta$  are evaluated according to Eqs. 1 and 2. The positions  $y_j$  and  $z_k$  can be defined in pixel coordinates such that they are directly mapped to the  $j, k$  indices. The x-dimension, being defined by the detector integration time is not affected by this transformation.

Linear interpolation is chosen as the initial algorithm for evaluating the modeled at-sensor radiance in the spatial direction, while standard spectral convolution using the detector pixels spectral response curves is used in spectral dimension.

### 3.1.3. PSF Convolution

The effect of the PSF width variations is modeled by convolving the photon flux at detector with a 2-dimensional normalized Gaussian distribution taking the at-detector coordinates  $(y_j, z_k)$  corresponding to continuous pixel indices. Thus the PSF of the pixel  $(j, k)$  is calculated as

$$PSF_{j,k}(y_j, z_k) = \frac{1}{2\pi\sigma_j\sigma_k} \exp\left(-\frac{(y_j - j)^2}{2\sigma_j^2} - \frac{(z_k - k)^2}{2\sigma_k^2}\right) \quad . \quad (4)$$

It is characterized by its widths  $\sigma_j$  and  $\sigma_k$  in the two dimensions. These two parameters are assumed to be constant for columns  $j/k$  respectively for the standard forward modeling case.

### 3.1.4. Stray Light

Stray light in the instrument is light that reaches the detector on an undefined optical path. Thus it cannot be described with the instrument’s spectral and spatial calibration. It is assumed to be a constant fraction of the average radiance of all pixels:

$$L_s^{stray} = c_{stray} \frac{1}{N_j N_k} \sum_{j=1}^{N_j} \sum_{k=1}^{N_k} L_{s,j,k} \quad (5)$$

where  $c_{stray}$  is the factor determining this fraction of stray light and  $N_j$  and  $N_k$  is the number of pixels in both directions. It is one of the calibration parameters of the instrument.

## 3.2. Bad Pixels

Bad pixels are expected to affect APEX image quality, since approximately 0.5 to 2% of all detector elements (i.e. 1500–6000 elements) may be defective. A simple forward model for bad pixel can be formulated analogous to the later Eq. 11, where an arbitrary gain  $G_{bp}^{j,k}$  and dark current  $DC_{bp}^{j,k}$  is introduced:

$$DN_{0,bp}^{j,k} = \Delta t G_{bp}^{j,k} L_s^{j,k} + DC_{bp}^{j,k} \quad (6)$$

The values of these factors may be anywhere between 0 and saturation level or could even be negative if detector readout errors are taken into account.

### 3.3. Radiometric Model

The radiometric forward model describes the optical and electronic transformation of the signal between detector input and data storage. Frown and smile optical aberrations are explicitly excluded in this part of the sensor model and are treated separately. Only the optical transmission is included as part of the radiometric model to let the correction of optical aberrations being done on normalized image data.

The conversion of radiance at sensor  $L_s$  to digital numbers  $DN$  can be split into individual processes as given in Figure 2. Hereafter, an attempt is made to merge the individual steps to a form which allows an efficient inversion of the radiometric measurement process. The equations below are given on a spectral band level and do not include any effects of spectral sampling and binning. The correction of these effects are part of the stray light and PSF correction procedure.

In a first step, the at sensor radiance is transmitted through the optics, registered by the detector and stored as electrons. This part may be written as:

$$q_d^{j,k} = \Delta t e_q^{j,k} \tau_{opt}^{j,k} L_s^{j,k}, \quad (7)$$

where  $e_q^{j,k}$  is the quantum efficiency of the detector elements,  $\tau_{opt}^{j,k}$  is the optical transmittance and  $L_s^{j,k}$  is the at-sensor radiance value resampled to the detector element  $j,k$ . The dark current adds to these electrons and an amplifier gain factor  $g_a$  applies such that

$$DN_0^{j,k} = q_d^{j,k} g_a^{j,k} + DC^{j,k}. \quad (8)$$

The dark current  $DC^{j,k}$  depends on the electron noise  $e_{dc}$  during readout, the integration time and amplification gain and can be given as:

$$DC^{j,k} = \Delta t e_{dc}^{j,k} g_a^j = \Delta t dc^{j,k} \quad (9)$$

The parameter  $G^{j,k}$  is now introduced as a total gain factor derived as the product of all multiplicative calibration constants between at-sensor radiance and  $DN$ -s per detector pixel, normalized by the integration time:

$$G^{j,k} = e_q^{j,k} \tau_{opt}^{j,k} g_a^j, \quad (10)$$

Using this factor, Eq. 8 may be rewritten as:

$$DN_0^{j,k} = \Delta t G^{j,k} L_s^{j,k} + DC^{j,k} = \Delta t \left( G^{j,k} L_s^{j,k} + dc^{j,k} \right), \quad (11)$$

where  $\Delta t G^{j,k}$  is the effective radiometric response factor (under the assumption of linear radiometric response functions). In addition to dark current, a smear during data readout applies at least to the visible part of the spectrum as further additive distortion. Its impact can be described as:

$$DN^{j,k} = \Delta t G^{j,k} L_s^{j,k} + DC^{j,k} + S^{j,k}, \quad (12)$$

where  $S^{j,k}$  is the smear on the detector while reading out.

An independent measurement of the charges  $q_d$  and the overlaid smear is not feasible using laboratory methods. Thus, the overall smear shall be parameterized using monochromatic detector readout tests. It is then assumed that the smear linearly depends on the raw  $DN_0$  values, which is sufficient as an initial assumption. However, iterative processes would make it possible to distinguish between smear and signal in the inversion process.

It is now assumed that the smear time  $\Delta t_s$  is constant for each detector element during frame transfer. The overall smear is now the summation of the individual contributions in all pixels where charges are transferred during readout:

$$S^{j,k} = \frac{\Delta t_s}{\Delta t} \sum_{j_s=1}^{n_j-1} DN_0^{j_s,k} , \quad (13)$$

where the digital measurement without smear distortions has been given in Eq. 11 and  $n_j$  is the number of pixels in readout direction.

The given simplification of Eq. 12 is appropriate as long as amplification and quantization of the detector readout  $q_d$  to digital numbers is assumed to be fully linear. Given the above equations, the parameters of the radiometric model can be reduced to the overall gain factor for each pixel  $j, k$  ( $G^{j,k}$ ), the time interval of readout smear in each detector ( $\Delta t_s$ ), and a dark current factor, given per second integration time ( $dc^{j,k}$ ). The variable integration time during data acquisition ( $\Delta t$ ) is a required instrument setting which is available from sensor configuration parameters.

The APEX instrument is configured such that freely programmable spectral binning allows for the selection of arbitrary combinations of spectral bands to be combined and stored to disk. Spectral binning can be radiometrically modeled as a simple summation of individual detector readouts in spectral dimensions:

$$DN^{j_b,k} = \sum_{j=b_1}^{b_2} DN^{j,k} , \quad (14)$$

where  $j_b$  is the new spectral band index after binning and  $b_1, b_2$  are the lower and upper limit of the binned original detector elements per binned band  $j_b$ , respectively.

#### 4. CORRECTION ALGORITHMS

Standard methods for radiometric calibration have been developed for various imaging spectrometers such as AVIRIS,<sup>7</sup> DAIS-7915,<sup>8</sup> CASI,<sup>9</sup> and others. More sophistication has been recently introduced into space sensor calibration such as MERIS<sup>10</sup> and MODIS.<sup>11</sup> Here, a smear model is introduced which allows for more exact calibration of smear effects. For MODIS, the correction of PSF variations is furthermore currently envisaged.<sup>12</sup>

Data processing is done in reverse order to the forward model, except for the optional spectral binning of the data values, which is not reversible. Thus, the index  $j_b$  in the following notation refers to a binned spectral band.

##### 4.1. Radiometric Calibration

Most current approaches for radiometric correction are based on assumptions of linearity and well-behaving systems. As such, standard radiometric data calibration procedures are usually based on Eq. 11. The inversion can then be done straightforward as:

$$L_s^{j,k} = \frac{DN_0^{j,k} - DC^{j,k}}{\Delta t G^{j,k}} . \quad (15)$$

For the APEX system, the binned calibration constants need to be calculated in calibration parameter retrieval first, resulting in  $DC^{j_b,k}$ ,  $G^{j_b,k}$  and  $S^{j_b,k}$ . The Eq. 15 is then rewritten. Radiometric data calibration of the APEX system requires the inversion of Eq. 12 and its inherent smear as given in Eq. 13. The at-sensor radiance  $L_s$  is derived as:

$$L_s^{j_b,k} = \frac{DN^{j_b,k} - DC^{j_b,k} - S^{j_b,k}}{\Delta t G^{j_b,k}} . \quad (16)$$

The readings not affected by smear (i.e.,  $DN_0$ ) of Eq. 13 can not be easily reconstructed without providing a preliminary or iterative smear correction scheme. However, assuming smear is low,  $DN_0$  can be replaced by the raw  $DN$  readings as a first order of approximation. Using Eqs. 9 and 13, the inversion model can then be written as:

$$L_s^{j_b,k} = \frac{1}{\Delta t G^{j_b,k}} \left( DN^{j_b,k} - \Delta t dc^{j_b,k} - \frac{\Delta t_s}{\Delta t} \sum_{j_s=1}^{n_j-1} DN^{j_s,k} \right). \quad (17)$$

One iteration on the smear correction part of this expression would increase accuracy and will be added in the future if smear is shown to be a major problem in data calibration.

## 4.2. Bad Pixel Replacement

A map indicating the position of bad pixels in the detector array is provided from sensor calibration. The values of defective pixels (Eq. 6) need to be replaced by valid realistic data. Bad pixel replacement is usually done by interpolation or nearest neighbor techniques. The following techniques are candidates for this procedure:

**nearest neighbor** the replacement of bad pixel by its nearest neighbors is not seen as being appropriate for creation of spectrally and spatially consistent detector frames.

**spatial interpolation** a pure spatial interpolation is appropriate for natural, spatially continuous scenes while it will surely fail over man-made areas.

**bilinear interpolation** this would be an easy straightforward model for bad pixel replacement within detector frames. However, it neglects the non-linear nature of spectral and spatial features.

**spectral interpolation** it is assumed that spectral correlation from band to band is much higher than spatial correlation in high resolution imaging spectrometer data. Thus, this is a favorite for further use.

An enhancement of the original data value has to be applied to pixels with low responsivity. In a first step, spectral interpolation is preferred for that process. The pixel values are completely replaced below a threshold responsivity. Interpolation is done within one detector frame (corresponding to one image line) in the spectral direction using the nearest neighbor responsive pixels. The image radiance is interpolated to the pixel position to obtain the bad pixel corrected image radiance :

$$L_s^{j_b,k} = s_{tr}^k \left( w_1 L_s^{j_b,k_1} + w_2 L_s^{j_b,k_2} \right), \quad (18)$$

where  $k_1$  and  $k_2$  are the closest responsive pixels per image row in both directions. The weighting factors  $w_1$  and  $w_2$  are derived as simple linear interpolation factors. The spectral shape factor is derived as the ratio on a default at-sensor radiance curve  $L_s^{def}$  between the spectral pixel to be replaced and the two reference pixels as:

$$s_{tr}^k = \frac{L_s^{def,k}}{w_1 L_s^{def,k_1} + w_2 L_s^{def,k_2}} \quad (19)$$

For higher accuracy, this replacement should be repeated after atmospheric correction to avoid the effects induced by sharp atmospheric and solar absorption features. However, such interpolated values may not meet the goals in radiometric calibration accuracy in any case. As a consequence, the bad pixel map will be provided to the end users to allow the exclusion of bad pixels during higher level processing.

### 4.3. Optical Calibration

During processing, the nominal wavelength  $\lambda$  and across-track angle  $\theta$  coordinates need to be specified for each pixel. This final data calibration step is mainly performed by a coordinate transformation, cf. section 4.3.2.

In order to correct for smile and frown, the observed radiance is resampled in the wavelength  $\lambda$  and across-track angle  $\theta$  directions, see section 4.3.3. The smoothing due to the width of the PSF is not inverted during the processing since such a deconvolution would introduce unwanted a priori knowledge into the observation implicitly. The calibration coefficients needed for processing are the parameters for deriving  $y_j(\lambda, \theta)$  and  $z_k(\lambda, \theta)$  and the fraction of stray light  $c_{stray}$ .

#### 4.3.1. Stray Light Correction

In order to correct for stray light, the stray light contribution is calculated according to Eq. 5 from the stray light calibration coefficient  $c_{stray}$  and the at detector radiances. Then the stray light is deduced from the at detector radiances. The approximation of using the observed radiances at detector for the stray light calculation is valid since  $c_{stray} \ll 1$ .

After stray light correction, PSF correction would be a possible next calibration step. Because the spatial PSF is expected to be stable across track, such correction is not part of the standard implementation but bears consideration for further development.

#### 4.3.2. Coordinate Transformation

The coordinate transformation from  $(\lambda, \theta)$  to  $(y_j, z_k)$  is parameterized with a 2-dimensional polynomial analogous to section 3.1.1:

$$y_j(\lambda, \theta) = a_0^j + a_1^j \lambda + a_2^j \theta + a_3^j \lambda^2 + a_4^j \theta^2 + a_5^j \lambda \theta \quad (20)$$

$$z_k(\lambda, \theta) = a_0^k + a_1^k \lambda + a_2^k \theta + a_3^k \lambda^2 + a_4^k \theta^2 + a_5^k \lambda \theta \quad (21)$$

It should be noted that  $y_j(\lambda, \theta)$   $z_k(\lambda, \theta)$  are continuous functions referring to the pixel coordinates on detector.

The parameterizations in Eqs. 20,21 and Eqs. 1,2 need to be chosen such that one set of equations is the inverse of the other. After the characterization of the real instrument, other parameterization may be substituted for the polynomials. The parameters  $a_0^j \cdots a_{J-1}^j$  and  $a_0^k \cdots a_{K-1}^k$  with  $J = K = 6$  for the choice of Eqs. 20,21 of the parameterization are the calibration coefficients for the optical data calibration.

#### 4.3.3. Radiance Resampling

Using the above formalism, arbitrary sets of  $\lambda, \theta$  duplets may be chosen for the resampling. However, in order to minimize smoothing effects of the interpolation in Eq. 22 the pairs shall be chosen such that they are as close as possible to the  $\lambda, \theta$  values of the detector pixels. At the same time the duplets shall define a grid with constant  $\lambda$  values in one dimension and constant  $\theta$  values in the other.

The  $\lambda$  and  $\theta$  values are chosen by averaging over all  $\lambda(j_b, k)$  and  $\theta(j_b, k)$  values for constant values of  $j_b$  and  $k$ , respectively.

The calibrated radiance is given in a matrix with specified  $j_b$  and  $k$  pixel index values. It is used as a look-up table (LUT) for evaluating the radiance at sensor for the targeted  $\lambda$  and  $\theta$  values, by averaging over a number of binned pixels  $N_b$  as given in Eq. 14:

$$L_s(\lambda, \theta)_b = \frac{1}{N_b} \sum_{j=b_1}^{b_2} L_s(y_j(\lambda, \theta), z_k(\lambda, \theta)) \quad , \quad (22)$$

where  $y_j$  and  $z_k$  are evaluated according to Eqs. 20, 21. This is analogous to Eq. 3, but includes the summation of binned spectral bands.

Bilinear interpolation is chosen as the initial algorithm for derivation of the values  $L_s(y_j(\lambda, \theta), z_k(\lambda, \theta))$ . Possible choices for an optimized version include cubic, thin plate spline and triangulation algorithms.

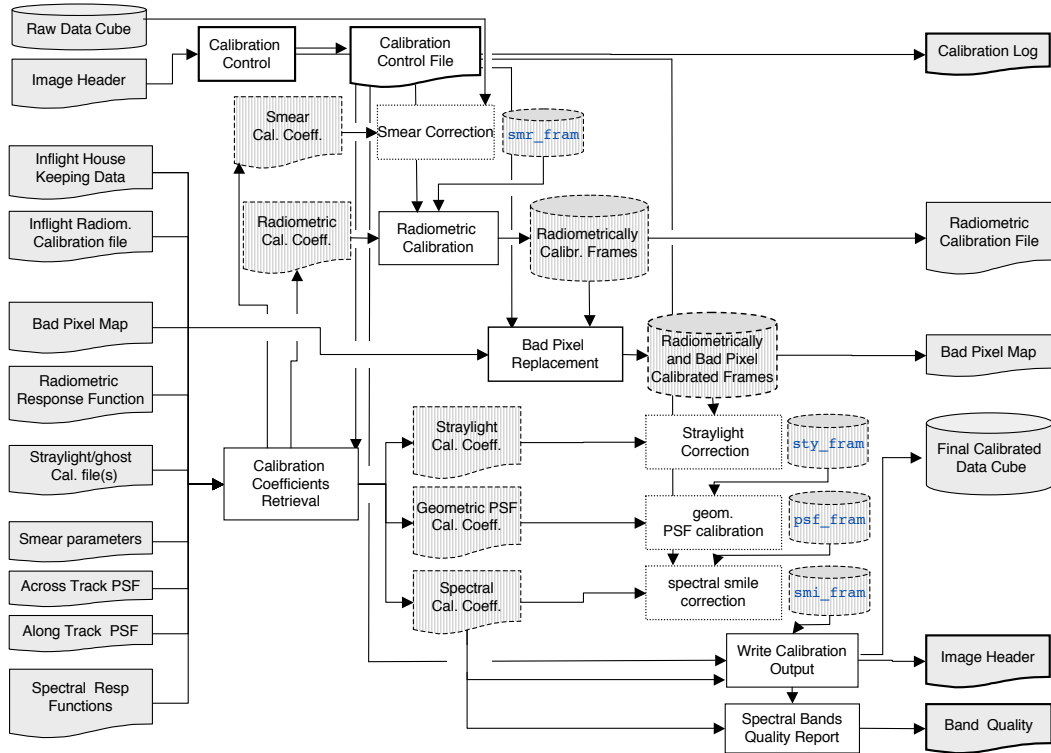


Figure 2. Level 1 implementation flow chart.

## 5. IMPLEMENTATION

All data calibration steps are performed in the Level 1 processing chain as depicted in Figure 2. The main task is the conversion of the scene from digital numbers to radiance values  $[W/(m^2 sr nm)]$  by applying the corrections for electronic, radiometric, and optical distortions. The processing is done in reverse order of the data acquisition process, i.e. the order of processing is first electronic, then radiometric, and finally optical effects. Bad pixels are replaced after radiometric data calibration since the replacement requires calibrated pixel neighbors for interpolation.

### 5.1. Calibration Coefficients Retrieval

Standardized calibration coefficients are created as the first step of each calibration process. They are combined from sensor calibration measurements resulting in spectral, geometric, and radiometric response functions for each detector element. A calibration data model underlies this creation process, simulating the temporal change of the sensor characteristics during the data acquisition phase. This model is described in detail in this issue by Kaiser et al.<sup>13</sup>

### 5.2. Radiometric Calibration

The acquired data is affected by smear effects given by the electronic data acquisition process. These smear effects (along with potential effects of the A/D conversion) have to be corrected first on the DN level of the data. Afterwards, the radiometric calibration corrects the overall sensor response following Eq. 17. This calibration step is done on a per-pixel basis using calibration constants in image frame dimensions.

### 5.3. Bad Pixel Replacement

The replacement of bad pixels is the last step in radiometric calibration, where a “best guess” of the measurement in defective detector pixels is reconstructed from neighboring pixels. The interpolation rules are supported by a standard LUT for at-sensor radiance signatures. The bad pixel map is provided to the end users to allow the exclusion of bad pixels during higher level processing.

## 5.4. Optical Effects Correction

The combination of all optical effects in the focal plane can be described as an overall convolution function. This function includes PSF variations, frown and smile distortions, optical channel mis-registration, ghost images and stray light effects. Three major steps are identified for the correction of optical effects: first the stray light is subtracted from the calibrated values. This step will have to include correction for ghost images if such are determined to be a significant part of the image distortions (currently, ghost images are not expected to be a significant problem in the APEX instrument).

The correction for variations of the PSF could be done by degrading all pixel values to the broadest PSF per detector line, using convolution methods (this step is not implemented for standard processing since stable PSF values are expected). The last step of optical corrections is the coordinate transformation to correct for smile and frown effects. This step being computationally intensive will be optional or may even be omitted if the instrument specifications can be kept at less than 0.2 pixels of distortions.

## 5.5. Processor Outputs

After processing, the delivered Level 1B data includes the following processed information:

**Calibrated Image Cube** BIP or BSQ formatted calibrated image cube, including ENVI formatted header file,

**Band quality report** report about the spectral and radiometric quality for each spectral band, including noise and calibration information,

**Bad pixel map** map describing the pixels which had to be replaced from neighbor values or had been treated separately in either fashion,

**Calibration processor parameters and log file** log and parameters which were finally applied to the pixel values for retrieval of radiance in relation to original measurements (including e.g. gain and offset), and

**Transformed position and attitude** synchronized and geographically transformed position and attitude data per image line/frame.

In addition, selected Level 0 products such as campaign description, quicklooks, or consistency reports are part of the distributed data.

## 6. CONCLUSIONS AND OUTLOOK

A concept and implementation approach has been presented for the APEX data calibration process. It includes the description of the transition between object space, image space and detector space as well as its inversion. A complete yet simple forward model of the APEX data acquisition process has been defined and a prototype inversion process depicted.

The treatment of the image data in the APEX processor is defined in order to allow efficient and reproducible handling. The data flow of the level 1 calibration process is defined in detail. It includes procedures for radiometric data calibration, bad pixel replacement and the correction of optical aberrations. The processor implementation will focus now on the evolutionary prototyping of this inversion process by first testing the basic implementation as presented. This code will help identifying the most time-critical processing steps and then prototyping selected additional options in the inversion process.

Since, in general, re-sampling from one coordinate system to another at the same resolution is a lossy process, there are many re-sampling algorithms to be evaluated depending on which characteristics you want to maximize/minimize. The crudest is nearest neighbor which is the simplest and least computationally expensive algorithm. Bilinear interpolation is a slightly better algorithm as it makes the output spatially smoother but spectrally perturbs the resulting image in a way that can be undesirable for many applications. An improved method could use cubic convolution. Instead of a mere linear interpolation of single nearest neighbors, a slightly larger neighborhood or convolution kernel is selected and analyzed in order to more precisely synthesize new

values depending on weighted influences of neighboring pixels. The effect of these various interpolation method on the calibration process needs to be further analyzed in future development work.

The presented calibration concept will be pursued during the operational phase of the APEX instrument, monitoring possible upgrades or degradations of the system. The open architecture of the processor allows enhancements to the processor to be done on a regular basis in response to the increasing knowledge of the APEX system's stability and performance.

## ACKNOWLEDGMENTS

This work has been carried out under support of ESA/ESTEC contract No. 15449/01/NL/SFe.

## REFERENCES

1. K. Itten, M. Schaepman, L. De Vos, L. Hermans, H. Schlaepfer, and F. Droz, "APEX - Airborne Prism Experiment a new concept for an airborne imaging spectrometer," in *3rd Int. Airb. Remote Sens. Conf. and Exh.*, **Vol. I**, pp. 181–188, ERIM International Inc., (Copenhagen, DK), 1997.
2. M. Schaepman and et.al., "APEX: Current status of the airborne dispersive pushbroom imaging spectrometer," in *Sensors, Systems, and Next Generation Satellites IX*, H. S. R. Meynart, S.P. Neeck, ed., **this issue**, SPIE, (Barcelona, SP), 2003.
3. P. Mouroulis, R. O. Green, and T. G. Chrien, "Design of pushbroom imaging spectrometers for optimum recovery of spectroscopic and spatial information," *Applied Optics* **39**(13), pp. 2210–2220, 2000.
4. D. Schläpfer, M. Schaepman, S. Bojinski, and A. Börner, "Calibration concept for the Airborne Prism Experiment (APEX)," *Can. J. of Remote Sens.* **26**(5), pp. 455–465, 2000.
5. D. Schläpfer and R. Richter, "Geo-atmospheric processing of airborne imaging spectrometry data. part 1: Parametric ortho-rectification process," *Int. J. Remote Sens.* **23**(13), pp. 2609–2630, 2002.
6. H. Kieffer, "Detection and correction of bad pixels in hyperspectral sensors," in *Imaging Spectrometry IV*, S. Shen, ed., **Vol. 2821**, pp. 93–108, SPIE, (Denver, CO), 1996.
7. T. Chrien, R. Green, and M. Eastwood, "Accuracy of the spectral and radiometric laboratory calibration of the Airborne Visible/Infrared Imaging Spectrometer (AVIRIS)," in *Im. Spec. of the Terrestrial Environment*, G. Vane, ed., **Vol. 1298**, pp. 37 – 49, SPIE, (Orlando, FL), 1990.
8. P. Strobl, A. Müller, D. Schläpfer, and M. Schaepman, "Laboratory calibration and in-flight validation of the digital airborne imaging spectrometer DAIS 7915," in *Alg. for Multispectral and Hyperspectral Im. III*, **Vol. 3071**, pp. 225–236, SPIE, (Orlando, FL), 1997.
9. A. Wilson, W. Mockridge, and M.-C. Robinson, "Post-processing to achieve radiometric and geometric correction of ATM and CASI data," in *3rd Int. Airb. Remote Sens. Conf. and Exh.*, **Vol. I**, pp. 447–454, ERIM International Inc., (Copenhagen, DK), 1997.
10. M. Rast and J. L. Bezy, "ESA's Medium Resolution Imaging Spectrometer (MERIS): Mission, system and applications," in *Im. Spec. of the Terrestrial Environment*, G. Vane, ed., **Vol. 1298**, pp. 114 – 125, SPIE, (Orlando, FL), 1990.
11. B. Guenther, D. Godden, X. Xiong, E. Knight, S.-Y. Qiu, H. Montgomery, M. Hopkins, M. Khayat, and Z. Hao, "Prelaunch algorithm and data format for the level 1 calibration products for the EOS-AM1 Moderate Resolution Imaging Spectroradiometer (MODIS)," *IEEE Trans. on Geosc. and Remote Sens.* **36**(4), pp. 1142–1151, 1998.
12. F. Rojas, R. Schowengerdt, and S. Biggar, "Validation of the on-orbit modulation transfer function for the Moderate Resolution Imaging Spectroradiometer (MODIS-AM) using on-orbit calibration data and high contrast imagery," in *Proc. IGARSS 2002*, **Vol. II**, pp. 973–975, IEEE, (Toronto, CA), 2002.
13. J. Kaiser, D. Schläpfer, J. Brazile, P. Strobl, M. Schaepman, and K. Itten, "Assimilation of heterogeneous calibration measurements for the APEX spectrometer," in *Sensors, Systems, and Next Generation Satellites IX*, H. S. R. Meynart, S.P. Neeck, ed., **this issue**, SPIE, (Barcelona), 2003.